AGU PUBLICATIONS

JGR

Journal of Geophysical Research: Space Physics

RESEARCH ARTICLE

10.1002/2017JA023916

**Key Points:**

- Ion frictional heating in the high-latitude ionosphere is studied by using incoherent scatter radars
- Anisotropic and non-Maxwellian ion velocity distributions are inferred from PFISR/RISR measurements
- Effect of Coulomb collisions on the ion distribution function is inferred from the derived ion temperatures

**Correspondence to:**
H. Akbari,
hakbari@bu.edu

**Citation:**
Akbari, H., L. V. Goodwin, J. Swoboda, J.-P. St.-Maurice, and J. L. Semeter (2017), Extreme plasma convection and frictional heating of the ionosphere: ISR observations, *J. Geophys. Res. Space Physics*, *122*, 7581–7598, doi:10.1002/2017JA023916.

Received 27 JAN 2017
Accepted 21 JUN 2017
Accepted article online 23 JUN 2017
Published online 13 JUL 2017



# Extreme plasma convection and frictional heating of the ionosphere: ISR observations

**H. Akbari[1], L. V. Goodwin[2], J. Swoboda[3], J.-P. St.-Maurice[2], and J. L. Semeter[1,3]**

[1]Center for Space Physics, Boston University, Boston, Massachusetts, USA, [2]Institute of Space and Atmospheric Studies, University of Saskatchewan, Saskatoon, Saskatchewan, Canada, [3]Department of Electrical and Computer Engineering, Boston University, Boston, Massachusetts, USA

**Abstract** Extremely elevated ion temperatures observed with the Poker Flat and Resolute Bay incoherent scatter radars in the *E* and *F* regions of the polar ionosphere are discussed. Our observations include one-dimensional, line-of-sight ion temperatures ($T_{i,1d}$) that at times can rise to up to ∼8000°K. While examining the accuracy of the derived temperatures is difficult due to the several potential sources of error and uncertainty, we find that at altitudes of ∼130–250 km the line-of-sight ion temperatures obtained at relatively small aspect angles (for instance, at 22.5° away from the magnetic field direction) are below the expected values for the average or three-dimensional ion temperatures ($T_i$). We find that this difference matches well with the theoretical expectation from anisotropic ion velocity distributions that emerge from polarization elastic scattering collisions between $NO^+$ and $N_2$. These results are therefore the clearest detection of anisotropic ion velocity distributions with the Poker Flat Incoherent Scatter Radar and Resolute Bay Incoherent Scatter Radar facilities. Moreover, at higher altitudes (> ∼300 km), where the resonant charge exchange collisions prevail, and for a very high ion temperature event ($T_i$ ∼ 8000°K), we observe that the incoherent scatter radar (ISR) spectra obtained at large aspect angles (e.g., 55°) look like those expected from non-Maxwellian plasma. At similar altitudes, the measured one-dimensional temperatures at an aspect angle of 22.5° are found to exceed the expected values from the frictional heating and resonant charge exchange collisions by about 1000°K. A portion of this offset is thought to reflect the role of Coulomb collisions.

## 1. Introduction

Incoherent scatter radars (ISRs) at high latitudes commonly detect ion temperatures in the *E* and *F* regions of the ionosphere that are substantially greater that their quiet time values [e.g., *Davies et al.*, 1999, 1995; *Hagan and Sipler*, 1991; *Baron and Wand*, 1983]. The elevated ion temperature events that are generally associated with ion frictional heating when the Lorentz force drives the ion gas through the neutral atmosphere [e.g., *Schunk et al.*, 1975; *St.-Maurice and Hanson*, 1982] are of interest from both the ionospheric and magnetospheric points of view. From the magnetospheric perspective the electric fields driving the $\boldsymbol{E} \times \boldsymbol{B}$ drifts are those within the magnetosphere that are directly mapped to the lower ionosphere. The flows could therefore be ionospheric signatures of magnetospheric processes such as flux transfer or reconnection [e.g., *Todd et al.*, 1986; *Lockwood et al.*, 1990; *Lyons et al.*, 2010; *Zou et al.*, 2009]. From the ionospheric point of view, frictional heating is one of the major mechanisms by which solar wind energy is deposited in the ionosphere. It plays an important role in the dynamics of the ionosphere and is related to a number of topics such as plasma transport, ion upflow, and chemistry in the ionosphere [*Zettergren et al.*, 2010; *Zettergren and Semeter*, 2012].

In addition to its significance in the context of large-scale magnetosphere-ionosphere dynamics, ion frictional heating also poses interesting microscale plasma physics questions. In the presence of a relative drift between the ion gas and the neutral atmosphere, $V_{in} = |\boldsymbol{V}_i - \boldsymbol{V}_n|$ (where $\boldsymbol{V}_i$ and $\boldsymbol{V}_n$ are the ion and neutral velocity vectors, respectively), ion-neutral collisions cause the departure of the ion velocity distribution from isotropic Maxwellian toward an anisotropic toroidal distribution [*St-Maurice and Schunk*, 1977, 1979]. Such a distortion of the distribution function is of critical importance to incoherent scatter radar (ISR) measurements of ionospheric parameters, since the standard ISR theory rests on the assumption of isotropic Maxwellian distributions for both electrons and ions. This effect has proved difficult to model and integrate into the ISR fitting procedure and is potentially a major source of error in estimating plasma parameters during periods of intense ion frictional heating [*Raman et al.*, 1981; *Lockwood et al.*, 1987; *Winser et al.*, 1987, 1989; *Moorcroft and Schlegel*, 1988; *Suvanto*, 1988].

In this paper we review Poker Flat and Resolute Bay ISR observations of elevated ion temperatures at high latitudes with the focus on the microscale plasma physics aspects of the observations. The goal of this manuscript is to summarize the observational features routinely detected by these radars, to comment on the validity of the derived temperatures, and to investigate and explore the advantages that such multibeam radar systems pose to study the anisotropic and non-Maxwellian nature of the ion distribution function when the ion-neutral differential flows are large.

The organization of the paper is as follows. In the next section and before presenting the experimental results, we briefly review the theoretical discussions on the effects of large $V_{in}$ and ion-neutral collisions on the ion distribution function and on the ISR spectrum. In section 3 we present Poker Flat Incoherent Scatter Radar/Resolute Bay Incoherent Scatter Radar (PFISR/RISR) data obtained from unique and the routinely performed "Themis" and "IPY" (International Polar Year) experiments. Section 4 includes discussions on the validity of the ion temperature measurements and general comments on the aspect angle dependence of the line-of-sight ion temperatures. Section 5 presents a summary and our conclusions.

## 2. Ion Distribution Function and ISR Analysis in the Presence of Large Ion-Neutral Differential Flow

Before getting into the details of nonthermal plasma production in the presence of ion-neutral collisions and large $V_{in}$, it is useful to revisit the definition of temperature. The true "three-dimensional" ion temperature, $T_i$, is defined from the second moment of the three-dimensional ion distribution function, $F(\boldsymbol{v})$ and, as such, is a measure of the average kinetic energy in three dimensions. Incoherent scatter radars, however, are only sensitive to the one-dimensional ion distribution function along the line-of-sight direction, i.e., $f(u, \hat{\boldsymbol{k}})$, which is defined according to equation (1):

$$f(u, \hat{\boldsymbol{k}}) \equiv \int F(\boldsymbol{v})\delta(u - \boldsymbol{v} \cdot \hat{\boldsymbol{k}})\mathrm{d}^3\boldsymbol{v} \tag{1}$$

Here $\hat{\boldsymbol{k}}$ represents a unit direction vector.

As a result, the temperature that an ISR derives is the one-dimensional, line-of-sight temperature, $T_{i,1d}$, which only represents the second moment of the one-dimensional distribution function along the line-of-sight direction. $T_{i,1d}$ is generally different from the three-dimensional temperature. However, for an isotropic Maxwellian distribution, $f(u, \hat{\boldsymbol{k}})$ remains Maxwellian with a single temperature $T_{i,1d} = T_i$ regardless of the line-of-sight direction.

In a magnetized plasma, provided that the ion gyrofrequency is greater than ion collision frequency (a condition that applies, for instance, in the $F$ region of the ionosphere), the presence of a magnetic field ensures that the distribution function remains gyrotropically symmetric—that is, symmetric with respect to the magnetic field axis. $T_{i,1d}$ therefore only depends on the angle between the line of sight and the magnetic field lines $\varphi$ (hereafter called the aspect angle) and as such may be replaced by $T_\varphi$. From the second moment of the distribution function it can be shown that [*Raman et al.*, 1981] for any gyrotropic form of $F(\boldsymbol{v})$

$$T_i = (T_\parallel + 2T_\perp)/3 \tag{2}$$

$$T_\varphi = T_\parallel \cos^2\varphi + T_\perp \sin^2\varphi \tag{3}$$

where $T_\parallel$ and $T_\perp$ are $T_\varphi$ for $\varphi = 0$ and $\varphi = \pi/2$, respectively.

Expectedly, the degree by which $F(\boldsymbol{v})$ deviates from isotropic Maxwellian is a function of the magnitude of the ion-neutral differential flow. For moderate relative drifts (i.e., $V_{in} < V_{n,\mathrm{th}}$, where $V_{n,\mathrm{th}} = \sqrt{\frac{2k_BT_n}{M_n}}$ is the neutral thermal velocity and $k_B$, $T_n$, and $M_n$ are the Boltzmann constant and neutral temperature and mass, respectively) $F(\boldsymbol{v})$ may be approximated by a bi-Maxwellian distribution where the one-dimensional distribution at any aspect angle $\varphi$ is Maxwellian but with a different temperature which continuously decreases from perpendicular to parallel directions. From equations (2) and (3) it follows that $T_\varphi$ equals $T_i$ at $\varphi = 54.7°$ regardless of the level of anisotropy; however, for $\varphi > 54.7°$, $T_\varphi$ approaches $T_\perp$ and is greater than $T_i$, whereas for $\varphi < 54.7°$, $T_i$ approaches $T_\parallel$ and is lower than $T_i$.

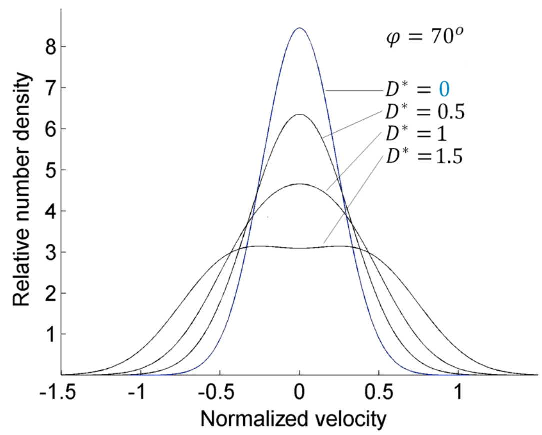


**Figure 1.** Line-of-sight one-dimensional ion distribution function at aspect angle of $\varphi = 70°$ for four values of $D^*$ approximately corresponding to $V_{in} = 0$, 1.1, 1.7, and 2.4 (km/s) (determination of $V_{in}$ from $D^*$ is only rough and is based on the results presented by *St.-Maurice et al.* [1976], *Lockwood et al.* [1989], and *Winkler et al.* [1992]).

For larger differential drifts ($V_{in} > V_{n,\mathrm{th}}$) the distribution function may severely deviate from Maxwellian, and this is in addition to its anisotropic form. From the ISR point of view the issue becomes concerning since the standard ISR analysis fails to describe non-Maxwellian plasmas. To account for this effect, a numerical or an analytical model capable of predicting the form of the distribution function is required. The accuracy of this model in turn relies on utilizing a realistic ion-neutral collision model.

An analytical approximation for the ion velocity distribution that applies to the O-O$^+$ plasma at altitudes $> \sim$250 km has been derived theoretically with the use of a simple Relaxation Collision Model (RCM) [*St-Maurice and Schunk*, 1979; *Raman et al.*, 1981]. The distribution function is given by equation (4) from *Raman et al.* [1981].

$$F(\boldsymbol{v}) = \frac{n_0}{\left(2\pi k_B T^*/M_i\right)^{3/2}} I_0\left(2D^*\left[|\boldsymbol{v}_\perp|^2/\left(2k_B T^*/M_i\right)\right]^{1/2}\right)\cdot \exp\left(-D^{*^2} - |\boldsymbol{v}|^2/\left(2k_B T^*/M_i\right)\right) \tag{4}$$

Here $n_0$, $M_i$, and $I_0$ are the electron density, ion mass, the modified Bessel function of order zero, respectively, $\boldsymbol{v}_\perp$ is the component of the velocity vector perpendicular to $\mathbf{B}$, and $D^*$ and $T^*$ are the two parameters of the distribution function. $D^*$ (also called the "perpendicular ion Mach number" by *Bernhardt et al.* [1998]—who discusses similar ion velocity distributions but in the context of space shuttle engine plumes in the ionosphere) is the shape parameter of the toroidal distribution and is responsible for the deviation of the distribution function from its Maxwellian form. $T^*$, on the other hand, has a meaning similar to temperature and represents the "width" of the distribution. Note that in equation (4) the functionality of the distribution function on $V_{in}$ has been indirectly incorporated via $D^*$. For instance, $D^* = 0$ (which represents zero deviation and therefore a Maxwellian distribution function) corresponds to $V_{in} = 0$ and it increases as the differential flow increases. The exact functionality of $D^*$ on $V_{in}$, however, is not known despite several theoretical and experimental studies [e.g., *Lockwood et al.*, 1989, and references therein].

Shown in Figure 1 are a few examples of the one-dimensional distribution function that emerges from the three-dimensional distribution function introduced above (see equation (30) of *Raman et al.* [1981] for the form of $f(u, \hat{\boldsymbol{k}})$ used here). Curves for $\varphi = 70°$ and four choices of $D^*$ are shown. It can be seen that for large values of $D^*$, $f(u, \hat{\boldsymbol{k}})$ flattens and starts to develop a minimum at the central point, which is also the position of the mean ion drift.

The ISR ion-line spectrum that arises from such distribution functions can be obtained via a procedure described by *Raman et al.* [1981]. Figure 2 shows a few example spectra for a range of $D^*$ and $\varphi$. As can be seen, the distortion of $f(u, \hat{\boldsymbol{k}})$ at large ion-neutral differential flows translates into departure of the ISR ion-line spectra from the well-known double-humped shape and a central peak develops between the two ion-acoustic shoulders. As seen here, the distortion of the ISR spectrum becomes more severe as the aspect angle increases.

In Figure 2 the value of $T_i$ has been kept constant regardless of the value of $D^*$ (i.e., $V_{in}$) in order to solely emphasize on the effect of the non-Maxwellian distribution on the ion-line spectrum. In reality, however, $T_i$ increases with $V_{in}$ due to frictional heating. Therefore, in Figure 3 we reproduce the spectra of Figure 2 while

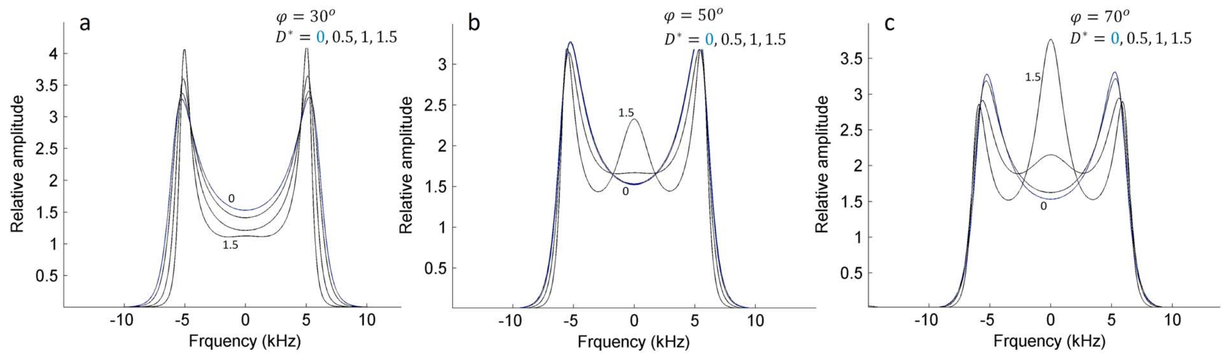


**Figure 2.** Theoretical ISR ion-line spectra associated with non-Maxwellian distributions based on the RCM solutions used by *Raman et al.* [1981]. Spectral calculations are shown as a function of aspect angle and $D^*$. In each case the spectra corresponding to $D^* = 0$ and 1.5 are tagged with their $D^*$ values and the other two spectra lie in between these. The spectra are calculated for $T_e = 2800$°K and $T_i = 1200$°K.

adopting reasonable values of $T_i = 1200$, 2000, 3000, and 4900°K associated with $D^* = 0$, 0.5, 1, and 1.5, respectively.

Via modeling the convection pattern and neutral winds in the ionosphere, *Lockwood and Fuller-Rowell* [1987] predicted that even during times of low geomagnetic activity ($Kp < 3$), the ion-neutral differential velocity often exceeds the neutral thermal velocity, and, as such, deviation of the distribution function from Maxwellian is a common property of the high-latitude plasma. They predicted that regions with the highest likelihood to contain non-Maxwellian distributions are the dawn sector of the auroral oval and the "throat region of the convection pattern," where the strong neutral winds of the afternoon sector meet the eastward ion flows of the morning sector. If not accounted for, the distortion of the ISR spectrum due to non-Maxwellian ion distribution could lead to severe errors in estimating the ionospheric parameters. Specifically, it could lead to overestimation of $T_i$ and underestimation of $T_e$ by up to a factor of 2 for severe deviations from Maxwellian at large aspect angles [*Raman et al.*, 1981; *Lockwood et al.*, 1987; *Winser et al.*, 1987, 1989; *Moorcroft and Schlegel*, 1988; *Suvanto*, 1988]. Miscalculating $T_r = T_e/T_i$ also leads to miscalculating the electron density since the total backscattered power is a function of both electron density and $T_r$.

The kinds of spectra predicted by *Raman et al.* [1981] based on the relaxation collision model were later verified in a number of ISR experiments with the European Incoherent Scatter (EISCAT) radars. *Lockwood et al.* [1987] measured nonthermal spectra similar to those shown in Figures 2 and 3 during a rapid ion flow event. Furthermore, *Winser et al.* [1987, 1989] showed that the variation of line-of-sight (one-dimensional) ion temperature with aspect angle was consistent with theoretical predictions. Later several studies quantitatively investigated the amount of error that would arise from fitting such nonthermal spectra by assuming a Maxwellian model [*Suvanto et al.*, 1989; *Suvanto*, 1990a]. These works ultimately led to incorporating Raman's model in the ISR fitting procedure at EISCAT facilities [e.g., *Suvanto et al.*, 1989].

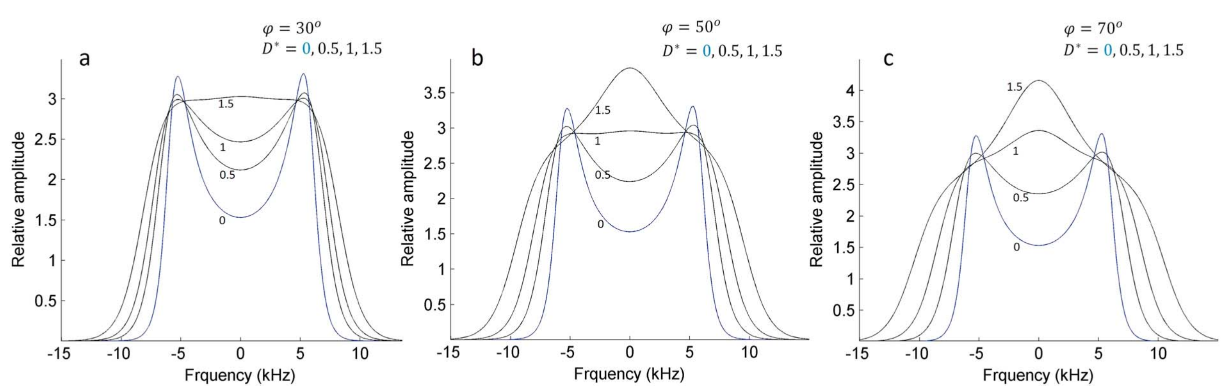


**Figure 3.** Spectra similar to those shown in Figure 2 but produced by adopting reasonable ion temperatures that take frictional heating into account. The adopted ion temperatures are only approximate as the goal is to make a qualitative point regarding the shape of the ISR spectra.

Despite its success in predicting a number of experimental observations, the Relaxation Collision Model (RCM) used in the *Raman et al.* [1981] calculations has shortcomings. This has been demonstrated by the Monte Carlo simulations developed by *Winkler et al.* [1992] which incorporate more realistic collision models, i.e., properly speed-dependent Resonant Charge Exchange (RCE) cross sections and a more accurate description of the ion-neutral polarization interaction and a proper mixing of RCE with polarization interactions. The improved calculations have shown that while the RCM can qualitatively predict the correct form of the distribution function, it exaggerates the amount of departure from Maxwellian [*Barakat et al.*, 1983; *Winkler et al.*, 1992]. For instance, ion velocity distributions similar to those shown in Figure 1 are obtained in the Monte Carlo simulations; however, they are obtained only for much larger ion-neutral differential flows. Furthermore, the distribution function employed by Raman does not allow any deviation from Maxwellian in the field-parallel direction, which is not always accurate.

Another important issue regarding these analytical results concerns the possible effect of plasma instabilities on the distribution function which is again not accounted for in the work of *Raman et al.* [1981]. It has been shown that for $V_{in}$ greater than a relatively low threshold (equivalently for $D^* > 1.5$) the distortions in the ion distribution are such that the one-dimensional distribution function for large aspect angles close to $\varphi \sim 90°$ develops a positive slope, giving rise to plasma instabilities and large-amplitude plasma waves [*St-Maurice*, 1978; *Suvanto*, 1987, 1990b] In fact, looking back at Figure 1 the positive slope can already be seen in the distribution function for $D^* = 1.5$. Note that the generated waves may not be observed directly by ISRs due to their field-perpendicular propagation direction and the geometry of most experiments. However, they are expected to affect the distribution function via quasilinear diffusion over a range of aspect angles around perpendicular to **B**.

Regardless of the shortcomings mentioned above, the non-Maxwellian analysis developed by Raman and even the standard ISR analysis based on Maxwellian ion distributions may still be used, provided that extreme attention is paid to the experimental parameters such as the magnitude of the differential flow and the aspect angle and altitude of observations. Extensive investigations of the ion distribution function and resulting ISR spectra based on Monte Carlo simulations are able to show in precise terms when the ISR spectral distortion is large enough to make a difference in the analysis. In particular, for the $N_2$-$NO^+$ plasma found at lower altitudes the distribution rarely, if ever, becomes unstable [*Winkler et al.*, 1992]. Furthermore, in the same region, unless $T_e >> T_i$, the calculations of the line-of-sight ion temperature based on a Maxwellian analysis of the spectrum are actually relatively precise (because of the small deviation of the ISR spectrum from the Maxwellian case, namely, $D^*$ typically less than 1 in those situations, as shown by *Winkler et al.* [1992]), so that only the anisotropic nature of the distribution function needs to be taken into account (as seen in spectra for which $D^* < 1$ when $T_e$ is not too large compared to $T_i$, e.g., in spectra shown by *Raman et al.* [1981]). The situation is different for the higher-altitude O-$O^+$ plasma under strong electric field conditions. In that case, the Monte Carlo approach enables us to produce a "region plot" to determine the transition for which a non-Maxwellian analysis is required and to address under what situations the analytical approach of *Raman et al.* [1981] can be considered to be reasonably accurate.

## 3. RISR/PFISR Observations of Elevated Ion Temperatures

The multibeam capability of the electronically steerable incoherent scatter radars that allow the readjustment of the beam direction in time scales below the radar's interpulse period (IPP) makes these radars powerful tools for three-dimensional imaging of the ionosphere [*Nicolls et al.*, 2004; *Semeter et al.*, 2009]. Such produced ionospheric maps often display ion flows associated with the ionospheric convection pattern or auroral arcs to coincide with regions of elevated ion temperature in the *E* and *F* regions [*Semeter et al.*, 2009]. The extreme values of the measured flows and temperatures provide an excellent opportunity to investigate several aspects of the nonthermal plasma discussed in the previous section. To this end, we have explored a large database of such events to determine which aspects of the theory can be directly observed in a typical experiment and the extent to which ISR data products are affected by them.

By investigating the daylong ionosphere-scanning ISR experiments, such as the "Imaging" experiments with RISR-N, one may identify elevated ion temperatures and also determine the time and location at which such events are more likely to occur. These many beam experiments (30 beams for the Imaging experiment), however, are not suitable for investigating the microscale aspects of nonthermal plasma since one consequence of employing a large number of radar beams is to reduce the number of pulses transmitted in each

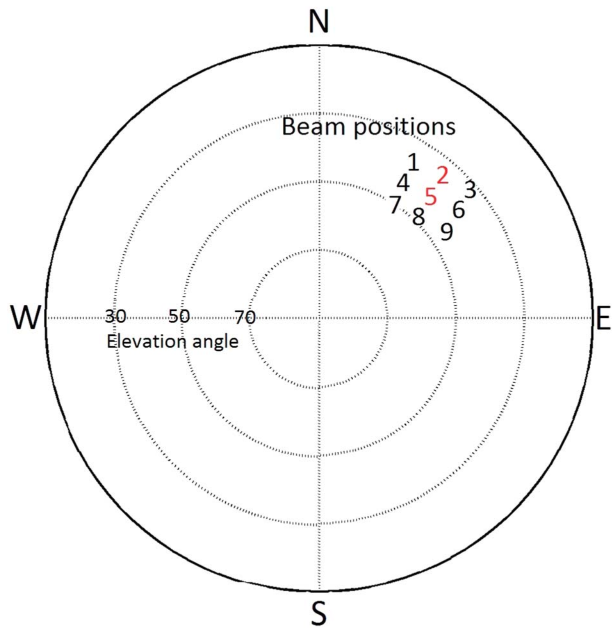


**Figure 4.** Radar beam positions for the RISR experiment run on 16 February 2015. The small elevation angles of the beams are suitable for detecting non-Maxwellian spectra. The magnetic zenith is close to an elevation angle of 90°.

direction within a fixed integration period and consequently to increase the statistical uncertainty in the measured spectra. One way to compensate for this is to adopt a longer integration interval—several minutes, for instance. This, however, is not favorable due to the high variability of the ionosphere during these periods. We therefore modified previous RISR experiments with the goal of obtaining an excellent data set that is suitable for our purposes. The modified mode consists of nine radar beams as summarized in Figure 4; however, two thirds of the transmitted pulses—14 out of any 21 consecutively transmitted pulses—are devoted to two beam directions only (beams 2 and 5). This is to maintain a good statistical certainty in measurements from these beams. In addition, the alternating code pulses that are routinely transmitted along with long pulses are removed in this mode. As such, we are able to obtain a far higher long-pulse repetition frequency than almost any typical experiment by RISR and PFISR. The point in including the remaining seven beams is to obtain a spatiotemporal context and to enable the determination of vector quantities such as the ion flow and the electric field. Below we present data obtained on 16 February 2015 with this mode.

Figure 5 shows the measured line-of-sight ion temperature in beam 2 as a function of time and altitude. Right around 18:20 UT the ion temperature at 320–450 km rapidly increases from below 2000°K to temperatures around and above 8000°K. The event lasts for about 20 min. This rapid increase in the ion temperature is associated with a rapid field-perpendicular ion flow with a velocity of ∼4 km/s. In Figure 6 we show line plots of the ion ($T_{i,1d}$) and electron temperatures as well as line-of-sight ion velocity through the elevated ion temperature feature. Here we have overplotted the data from three altitude intervals centered at 370, 393, and 416 km and as such the plots tend to represent the maximum/minimum rather than the average values. A pronounced behavior in Figure 6 is the drop in the retrieved electron temperature simultaneous with the increase in the retrieved ion temperature. This anticorrelation between retrieved $T_e$ and $T_i$ is likely a result of error in the ISR analysis and possibly a signature of non-Maxwellian ion distribution [*Winser et al.*, 1987, 1989; *Moorcroft and Schlegel*, 1988].

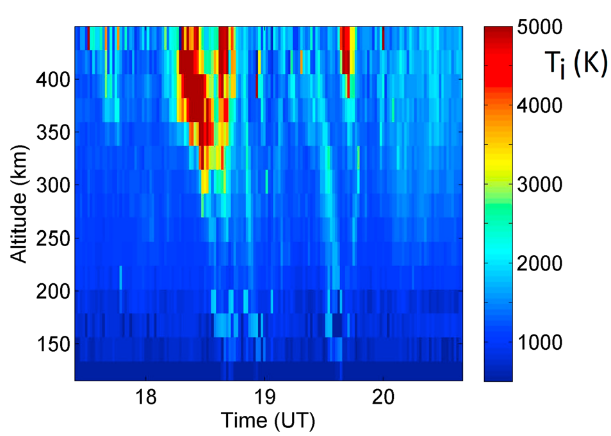


**Figure 5.** Retrieved line-of-sight ion temperature as a function of time and altitude, obtained on 16 February 2015, from beam 2 at an aspect angle of ∼55°. The integration period is 75 s during which 1785 pulses are transmitted. In the fitting procedure, 100% atomic oxygen has been assumed for the neutral composition at altitudes greater than 300 km.

In order to evaluate the accuracy of the fitted plasma parameters, it is important to closely examine the measured ion-line spectrum. Figure 7 shows the spectrum as a function of altitude for the case presented in Figure 5. Between ∼200 and 300 km a classic double-humped shape can be observed which is associated with daytime *F* region where the plasma density and

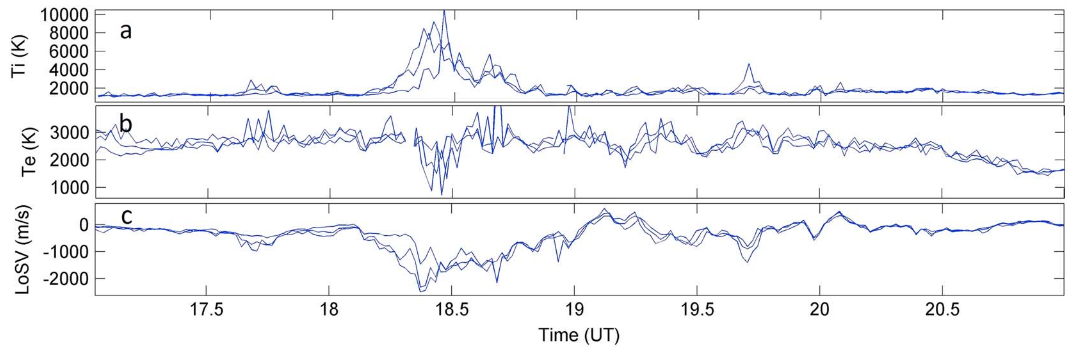


**Figure 6.** Line plots of the retrieved $T_{i,1d}$, $T_e$, and line-of-sight $V_i$ for the three altitude intervals centered at 370, 393, and 416 km, through the elevated ion temperature feature shown in Figure 5.

the electron-to-ion temperature ratio are both high. The small offset in the spectrum with respect to zero frequency indicates a small line-of-sight plasma motion at these altitudes. At higher altitudes, however, several things happen. First, the backscattered signal power decreases due to the decreasing plasma density. Second, the spectrum shifts toward positive frequencies indicating large line-of-sight plasma flows toward the radar. Third, due to frictional heating, the ion temperature increases above the electron temperature, ion-acoustic shoulders widen due to increased Landau damping, and consequently, the spectrum flattens and deviates from the double-humped shape. It can be seen that despite the theoretical expectation for the ion distribution to severely deviate from Maxwellian and even though one possible signature of non-Maxwellian distribution has appeared in the form of anticorrelation between the electron and ion temperatures, the ISR spectrum may not be classified as a characteristic non-Maxwellian form solely based on visual examination. This is unlike the results published in several previous publications where an enhanced central peak was clearly observed in the spectrum [e.g., *Lockwood et al.*, 1987].

Figure 8 provides an explanation for how the ISR fitting procedure behaves when analyzing data from this event. In Figure 8a the blue curve is an example of a spectrum measured during the elevated ion temperature feature and the green and black curves are examples of theoretical fits that are produced by adopting a Maxwellian ion distribution. In Figure 8b the red curve is also a theoretical spectrum though obtained from Raman's model where the deviation of the distribution function from Maxwellian is allowed. The point of this figure is to illustrate the difficulty of the standard ISR analysis in producing a good fit to the measured spectrum without artificially decreasing the electron temperature. If we set the electron temperature to 2800°K—i.e., to its value at 18.2 UT, preceding the sudden increase in $T_i$—the best fit to the measured spectrum will be poor as shown with the green curve. Keeping $T_e$ constant and further increasing $T_i$ worsens

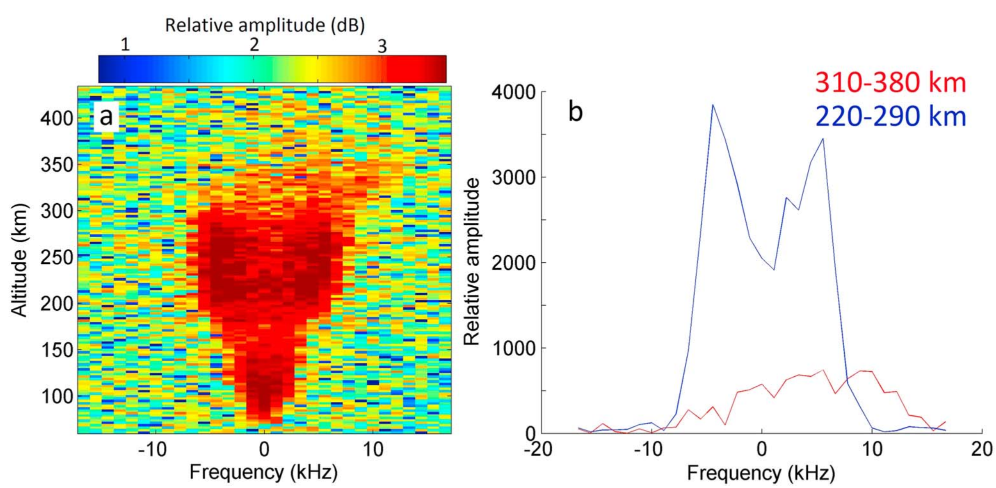


**Figure 7.** (a) Ion-line spectrum as a function of altitude from within the period of elevated ion temperature shown in Figure 5. The spectrum is produced by averaging over 30 s (714 pulses). (b) Line plots from Figure 7a averaged over 220–290 km and 310–380 km.

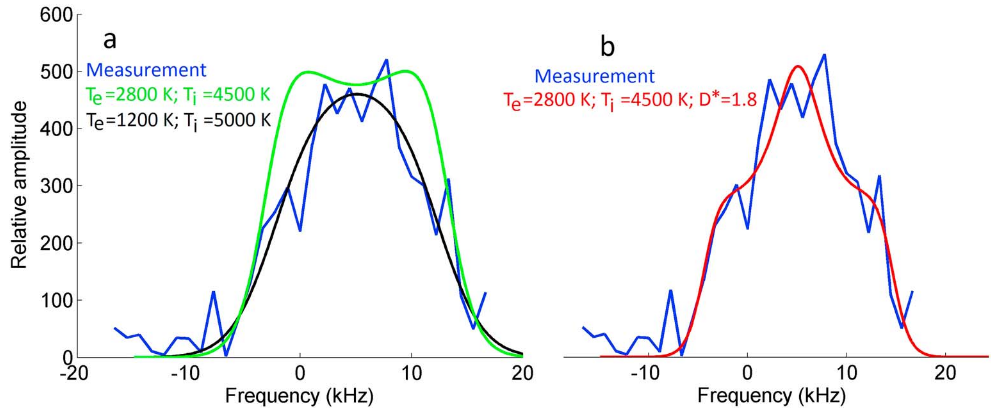


**Figure 8.** (a) Example measured and theoretical ISR spectra illustrating the quality of fit using a Maxwellian velocity distribution as opposed to the (b) non-Maxwellian spectrum of the type discussed in *Raman et al.* [1981].

the fit as the spectrum further widens. On the other hand, reducing $T_i$, although narrows the spectrum, may not produce a better fit as the central part of the spectrum deepens. An alternative, of course, is to increase $T_i$ and simultaneously decrease $T_e$ in which case a good fit may be achieved as shown with the black curve. This seems to be the reason for the anticorrelation of $T_e$ and $T_i$ in Figure 6. By allowing the non-Maxwellian effects in the fitting procedure, however, one can obtain a good fit (the red curve in Figure 8b) while maintaining the electron temperature at 2800°K yet increasing the ion temperature to higher values of ~4500°K. Note that in Figure 6, at times when the fitted ion temperature reaches to its highest values and the fitted electron temperature drops to values as low as ~1000°K, the estimated 1 sigma errors obtained from the standard ISR fitting procedure reach to values as large as 2000°K, 1200°K, and 200 m/s for $T_{i,1d}$, $T_e$, and $V_i$, respectively, indicating great uncertainty in the obtained parameters.

An important point that needs clarification regarding the comparison between the theoretical and experimental spectra in Figure 8 is the fact that the experimental spectrum is, to some degree, influenced by factors that are not considered in producing the theoretical spectra. Specifically, the smoothing effects of the lag ambiguity functions associated with the transmitted waveform or the receiver filter [*Raman et al.*, 1981] that are intrinsically included in the measured spectra are not incorporated in the procedure underlying the theoretical curves. Therefore, while our explanation above remains valid in a qualitative sense, a more robust procedure is required for a precise quantitative analysis. This will be discussed further in our final section.

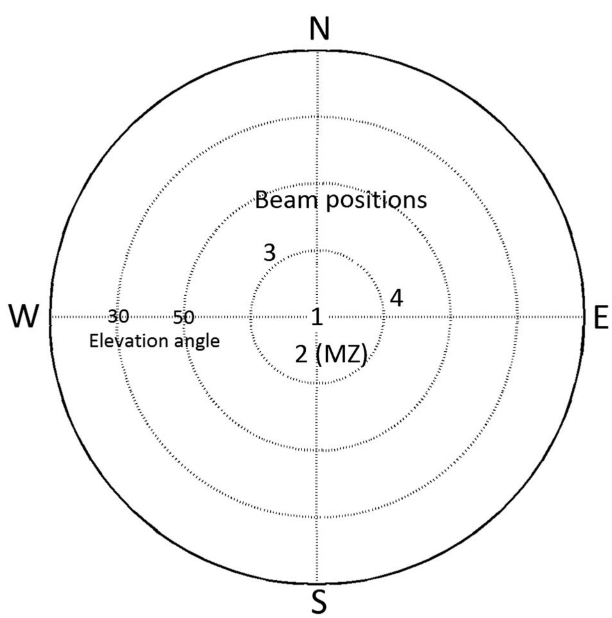


**Figure 9.** Radar beam positions for the IPY experiment by PFISR. Beam 2 is along the magnetic zenith.

Ion flows and elevated ion temperatures similar to those shown in Figures 5 and 6 are also regularly observed with the Poker Flat ISR. The daily operation and the amount of data gathered by this radar make it possible to analyze more events and to conduct statistical studies. To this end, we have searched the PFISR database obtained during the year 2012 and identified a large number of events where the ion temperature in the *E* and *F* regions was elevated. Two common programs that we have investigated for this study are the Themis and "International Polar Year (IPY)" experiments.

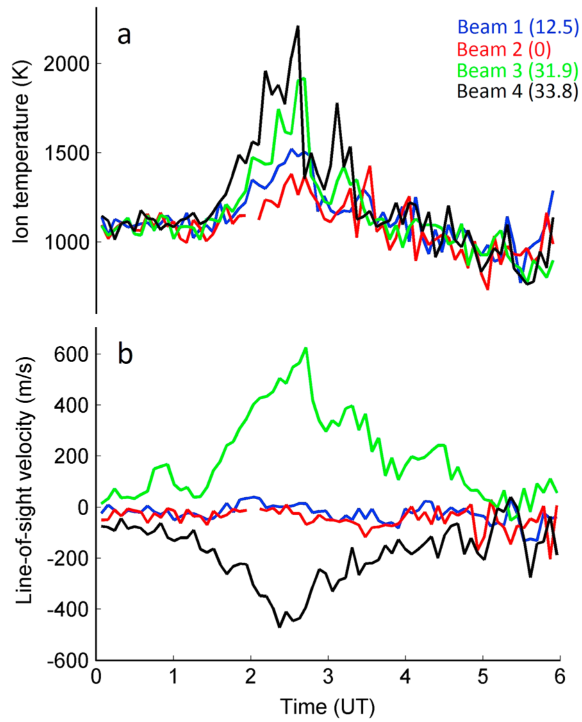


**Figure 10.** An example of the typical one-dimensional ion temperatures and line-of-sight velocities observed on 26 April 2012 in the IPY common program. The measurements are from ~300 to 420 km where the ion and neutral species are predominantly $O^+$ and O. Numbers in parentheses are the aspect angle for each beam.

Unlike the Imaging experiments, the IPY experiments consist of only four radar beams with relatively small aspect angles. These are the magnetic zenith, the vertical, and two side beams that each makes an aspect angle of ~33° (see Figure 9). Consistently observed in these experiments are elevated ion temperatures associated with westward and northwestward ion flows during local evenings. Figure 10 shows the one-dimensional ion temperature and line-of-sight ion velocities averaged between 300 and 420 km for each beam during one of such events. The magnitude of the line-of-sight velocity reaches to about 500–600 m/s at its peak in the side beams and decreases in the vertical and magnetic zenith beams as the observing aspect angle decreases. This is mainly due to the geometry of the experiment and the field-perpendicular direction of the flow.

Looking at the ion temperature, it can be seen that $T_{i,1d}$ also decreases with aspect angle and the temperature in the magnetic zenith and vertical beams are considerably lower than those in the side beams when the line-of-sight ion flows are large. Similar behavior is consistently observed in a large number of events. Since the different radar beams probe different parts of the ionosphere, which may not necessarily contain a homogeneous $V_{in}$, these measurements from different beams may not be directly used to study the aspect angle dependence of ion temperature and the anisotropic ion distribution in the presence of a large $V_{in}$.

However, a simple procedure, however, may clarify to what extent the differences in $T_i$ from different radar beams are due to inhomogeneous $V_{in}$. Provided that the ion-neutral frictional heating is strong, the ion energy balance equation reduces to [*St-Maurice and Schunk*, 1979]

$$T_i = T_n(1 + 2D'^2/3) \tag{5}$$

where $D' = V_{in}/V_{n,\mathrm{th}}$. Furthermore, for a bi-Maxwellian ion distribution and a given ion-neutral collision model, the partitioning coefficients $\beta_\parallel$ and $\beta_\perp$ may be defined such that [*St-Maurice and Schunk*, 1979]

$$\begin{aligned} T_\parallel &= T_n\left[1 + \beta_\parallel D'^2\right] \\ T_\perp &= T_n\left[1 + \beta_\perp D'^2\right] \end{aligned} \tag{6}$$

$\beta_\parallel$ and $\beta_\perp$ depend on the ion-neutral collision model and mass ratio and obey the relationship $\beta_\parallel + 2\beta_\perp = 2$. For the ion and neutral masses and electric fields appropriate for the observations presented in this study the calculated values for $\beta_\parallel$ and $\beta_\perp$ are 0.27 and 0.86 for resonant charge exchange model (applicable to $O^+$-O collisions at higher altitudes) and 0.52 and 0.74 for polarization elastic scattering model (applicable to $NO^+$-$N_2$ collisions at lower altitudes) [*Gaimard et al.*, 1998]. For conversion of the generalized cross sections in *Gaimard et al.* [1998] to the partitioning coefficients, see *St-Maurice and Schunk* [1979]. From the value of the line-of-sight ion temperature in beam 4 (1850–2150°K) and neutral temperature of $T_n = 1100$°K (determined from the ion temperatures at around 1 UT) we may approximate $D' = 1.01–1.12$ to the first order using equation (5). Now using equation (6) and the partitioning coefficients for the resonant charge exchange model, $T_\parallel$ is estimated 1477–1564°K, whereas the maximum value of measured $T_\parallel$ in Figure 10 is ~1320°K.

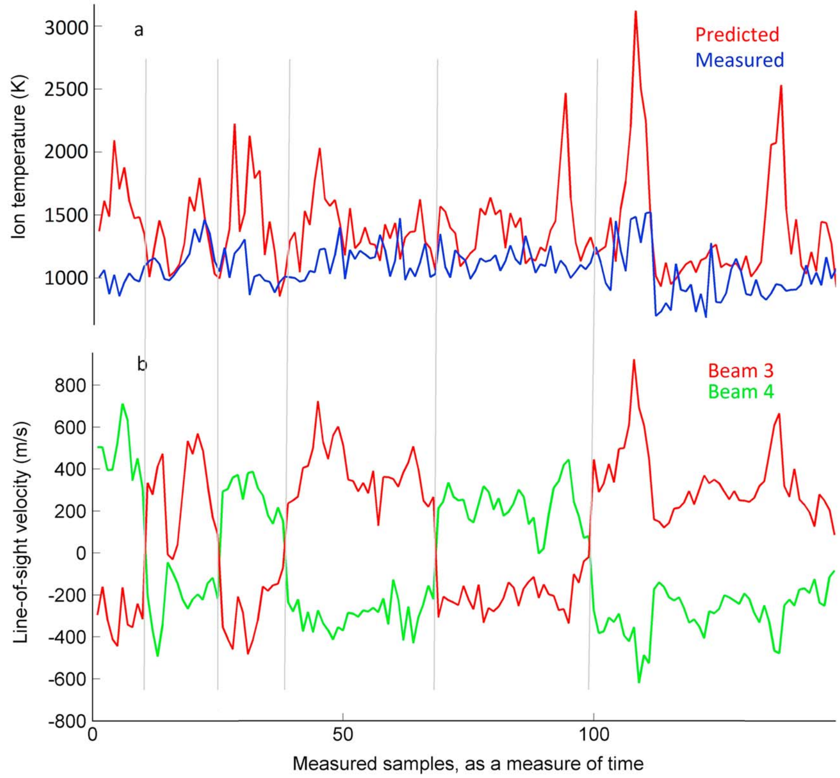


**Figure 11.** (a) The predicted and the measured $T_{\parallel}$ from six events (separated by the vertical gray lines) observed in IPY experiments. (b) Line-of-sight ion flows in beams 3 and 4 corresponding to the measurements shown in Figure 11a. Here the horizontal axis is in samples, each integrated for 5 min. Finally, the measurements are from ~300 to 420 km where the ion and neutral species are predominantly $O^+$ and O.

The unexpectedly high $T_{\parallel}$ events in the IPY experiments were not limited to the example provided in Figure 10. In the IPY experiments we found several events where the line-of-sight ion flows in beams 3 and 4 are relatively constant over the altitude range of 200–600 km for a period of time. Given the elevation angle of these beams, this may suggest that the flows are relatively constant in latitude. For such events it is possible to perform a similar analysis. Assuming a homogeneous $V_{in}$ and using equations (2) and (3) and the measured line-of-sight temperatures at two different aspect angles, i.e., $\varphi = 31.9°$ and 12.5°, we are able to estimate $T_{\parallel}$ and compare the results with the ion temperature measured in the magnetic zenith beam. Figure 11 shows the result of the comparison for a few selected events. As can be seen, the predicted $T_{\parallel}$ is far greater than the measured values. Furthermore, the lack of correlation between the two curves suggests that the inhomogeneity in $V_{in}$ is generally significant and masks the aspect angle dependence of the line-of-sight ion temperature.

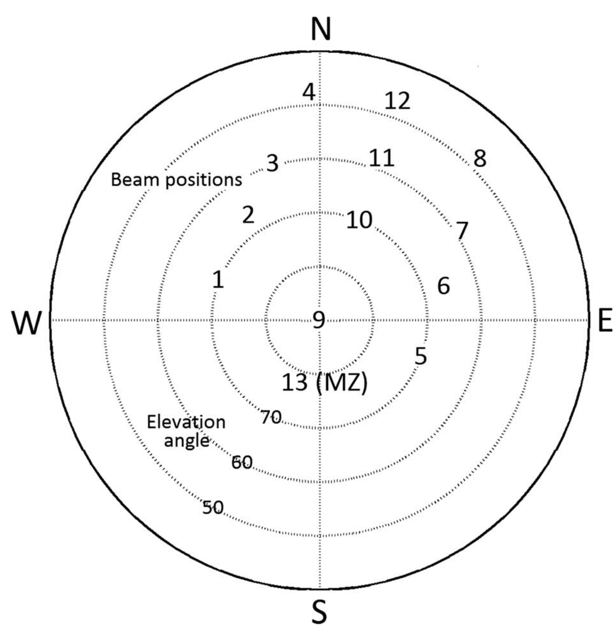


**Figure 12.** Radar beam positions for the Themis experiment by PFISR. Beam 13 is along the magnetic zenith.

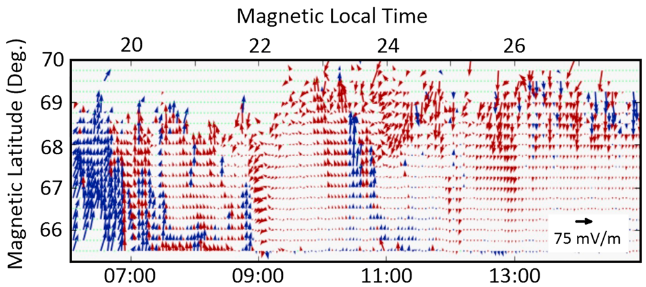


**Figure 13.** Altitude-averaged field-perpendicular electric fields obtained from the line-of-sight velocity measurements in the Themis experiment conducted on 3 March 2012. The colors indicate the direction of the east-west component of the electric field (blue for eastward and red for westward) and do not introduce additional information beyond the arrows.

In Themis experiments, 13 radar beams—including the magnetic zenith and vertical beams—are employed to form the pattern shown in Figure 12. This geometry covers a range of aspect angles from 0 to 55°. Figure 13 shows an example of the electric fields determined from the line-of-sight ion drifts in the 13 beams on 3 March 2012. Complementary to this figure is Figure 14 that shows the line-of-sight ion velocities as a function of altitude and time observed in beam 3. (Calculation of the horizontal vector velocities and electric fields from line-of-sight velocity measurements is a routine procedure for dvanced Modular Incoherent Scatter Radar (AMISR) radars; for discussions, see *Heinselman and Nicolls* [2008].) The main features of these plots—that were repeatedly observed in Themis experiments during 2012—are (1) northward electric fields (corresponding to westward ion flows) during local evenings (here more pronounced between 6 and 7 UT) which are associated with the duskside convection pattern and (2) rapid flow bursts similar to that at 10:30 UT which are more localized in latitude. Given the elevation angle of the radar beams, localization of ionospheric features in latitude translates into localization in altitude once observed in altitude-time format plots. The flow burst, therefore, appears in Figure 14 between ~250 and 450 km.

In order to perform a quantitative analysis on the events observed in the Themis experiments, we adopt the following procedure. We first identify an elevated ion temperature event in the ISR data. We then associate an average one-dimensional ion temperature and a line-of-sight velocity value to the prominent features within the identified period. The features should be visually obvious and last for at least two consecutive measurement samples (at least 4 min, depending on the integration time for one measurement sample). Furthermore, features that present a large variance or noise-like fluctuation in time are discarded. We believe that this procedure is appropriate as it may be the most common way of associating a value to an event and may facilitate the comparison between these and the previously published results. From the line-of-sight velocities we then estimate the field-perpendicular vector velocities using the elevation and azimuth angles of each radar beam and the overall coarse direction of the vector ion velocity. The latter is routinely determined as part of data processing for the AMISR radars.

One way of collectively presenting results from many events of the kind shown in Figure 14 is illustrated in Figure 15. Here the difference between the one-dimensional ion and neutral temperatures (i.e., $T_{i,1d} - T_n$) from about 30 events (each point represents a single event but is not necessarily from different days) is shown as a function of the simultaneously estimated field-perpendicular ion flows. For reasons that are discussed below, data points are symbol and color coded, based on the aspect angle and altitude of the observations.

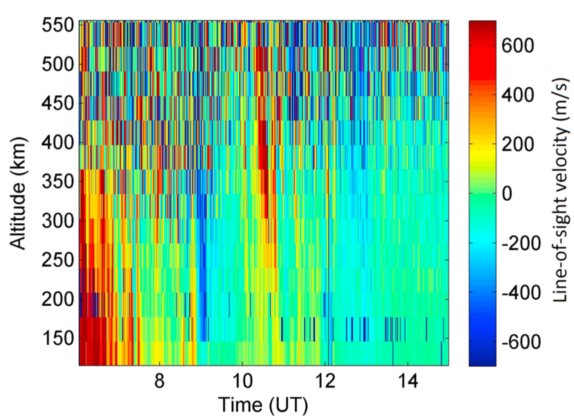


**Figure 14.** Line-of-sight velocity as a function of time and altitude obtained from beam 3 ($\varphi = 41.4°$) on 3 March 2012. Positive values indicate flows toward the radar.

The majority of the events shown in Figure 15 are obtained from the range gate that spans between ~130 and 250 km in altitude. This is the altitude range where the dominant ion species rapidly changes from molecular to atomic oxygen ions in a quiet, undisturbed ionosphere. During geomagnetically active periods the ion composition at these altitudes is subject to considerable variation and the

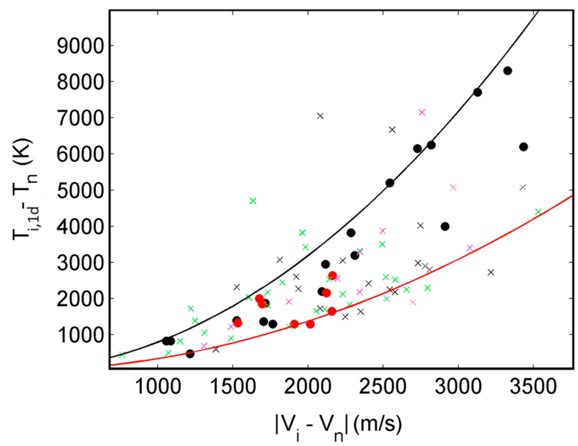


**Figure 15.** From the Themis experiments, measured one-dimensional ion temperatures as a function of the ion-neutral differential flow (or equivalently the ion flow, since $V_n$ has been assumed to be 0). Black and red circles represent measurements from ~130–250 km and ~300–400 km altitude ranges, respectively, obtained in beam 1 (aspect angle of 22.5°). Also, green, black, and purple crosses represent data points obtained in beams 2, 3, and 4 (i.e., aspect angles of 31.7°, 41.4°, and 53.7°, respectively). No color coding based on altitude is applied to these measurements. Also shown are the theoretical curves that illustrate the functionality of $T_{i,1d}(\varphi = 22.5°) - T_n$ on the differential flow. The black and red curves correspond to neutral composition ratios of 1/3 O and 2/3 $N_2$ versus 100% O, respectively. They are produced by adopting the partitioning coefficients for the polarization scattering and resonant charge exchange collision models, respectively.

output of general ionospheric models that are typically employed in the fitting procedure will not be accurate. There now exist several techniques to model and measure such variations of the ion composition [see *Zettergren et al.*, 2011, and references therein]. The PFISR Themis experiments utilize such techniques. Indeed, by inspecting the fitted ion composition during our events, we observe that the ion temperatures in the 130–250 km altitude range (including the black circles in Figures 15) are obtained by assuming ion compositions of +95% molecular ions, whereas the ion temperatures in the ~300–400 km altitude range (including the red circles) are obtained while assuming an ion composition of 100% atomic oxygen. As will be discussed further in section 4, the fitted compositions appear to be consistent with outputs of models that incorporate the effects of frictional heating and as such the measured ion temperatures are believed to be free of large errors that could be associated with inaccurate ion composition assumptions.

A further challenge in assessing the association of the ion temperature with a given electric field is that many of the events shown here are recorded during times when appropriate neutral atmosphere measurements from Fabry-Perot interferometers are not available. In the absence of these measurements, we obtain the neutral temperature from ISR measurements of ion temperature at quiet times prior to the high $T_i$ events when no significant $V_i$ is present, and we furthermore assume that $V_n = 0$. Although the latter assumption may be far from accurate for the most intense events (as discussed below), the benefit of this is that now the measured field-perpendicular ion flows may be labeled as the differential ion-neutral flow and this enables us to compare the measurements with theory.

Overplotted in Figure 15 are the theoretical curves based on equations (2)–(6), which show the functionality of $T_{i,1d}(\varphi = 22.5°) - T_n$ on the differential flow for two choices of neutral composition. It can be seen that the measured line-of-sight temperatures from beam 1 (aspect angle of 22.5°) do somewhat follow the theoretical curves. These measurements will therefore provide the opportunity to experimentally verify the validity of the theoretically derived partitioning coefficients discussed before. Properly addressing this, however, requires a close attention to a number of assumptions involved in our analysis, such as the adopted ion and neutral compositions, neutral wind, and the possible sources of error and uncertainty which will be discussed in the next section.

In Figure 15, unlike measurements from beam 1, measurements from beams 2, 3, and 4 do not illustrate a well-defined functionality on the differential flow. This is due to the large scatter in data points which also buries the aspect angle dependence of the line-of-sight ion temperature in these measurements. The scatter in data from these beams is most likely due to the increased error in the estimated $V_i$. In deriving the ion vector velocities from the line-of-sight values, there are several sources of inaccuracy; the most important of these is the possible error in the exact direction of the field-perpendicular flows. Given the geometry of the Themis experiment and the common zonal direction of the flows, this error is expected to be minimal for beam 1 and to affect increasingly strongly the analysis as the projection angle between the flow and radar beam increases.

In Figure 15 while the error bars associated with measurements have been removed for the sake of readability, the scatter in the data points may be used as a proxy for error estimates. The standard ISR analysis does provide error estimates for the fitted parameters. Such error estimates, however, are not necessarily reliable in our events since the procedure does not take into account the several sources of error discussed before. Nevertheless, and in order to provide a better understanding on the significance of the obtained results, we will present the ion temperature error estimates obtained from the ISR fitting procedure in the next section when we revisit a portion of the data shown in Figure 15.

## 4. Discussion

The threshold at which the ion distribution begins to deviate from Maxwellian and bi-Maxwellian depends on the ion species and the nature of collisions between ions and neutrals but is generally expected for $V_{in} > V_{n,\mathrm{th}}$ for the ionospheric *F* region. Based on in situ distribution measurements, *St.-Maurice et al.* [1976] showed that the distribution function for atomic oxygen ions was already non-Maxwellian when the frictional heating was enough to increase the ion temperature to ~3000°K in the upper *F* region. In our ISR data, although mostly obtained from lower altitudes, the inherently one-dimensional ion temperatures span from below 3000°K to far greater values, and, as such, the measurements should cover the transition region and reflect both thermal and nonthermal distributions. This leads us to attempt for the first time in multibeam PFISR and RISR experiments to identify the characteristic non-Maxwellian ISR spectra. We mean by this spectra with the pronounced central peak along with the ion-acoustic shoulders that are theoretically predicted and at times measured by the EISCAT radars [e.g., *Lockwood et al.*, 1987]. However, unambiguous detection of such spectra by visual examination of the data has proven to be challenging.

For the example shown in Figure 7 a toroidal distribution function is expected from the value of the estimated field-perpendicular ion flow. Furthermore, the large angle between the observing beam and the magnetic field lines is suitable for detecting the non-Maxwellian spectra. Yet despite the obvious anticorrelation between the measured electron and ion temperatures, the spectra may not be classified as non-Maxwellian by visual examination. Such an inconsistency could arise from a combination of several factors. First, at times when the ion temperature significantly exceeds the electron temperature, the ISR spectrum for a Maxwellian distribution is no longer the classic double-humped shape shown in Figure 2a. Due to the increased Landau damping, the ion-acoustic shoulders broaden and the spectrum approaches a single broad peak centered at zero frequency. As such, it becomes increasingly difficult to distinguish Maxwellian- and non-Maxwellian-type spectra. Furthermore, as explained by *Raman et al.* [1981], instrumental effects associated with the final pulse widths and the receiver filter tend to smooth out the non-Maxwellian features in the measured spectra. Finally, in an ISR experiment that employs a large number of radar beams and for situations where the scattered power suffers from a comparatively low signal-to-noise ratio, the slight differences between Maxwellian and non-Maxwellian spectra may be covered by the noise-like spectral fluctuations in the measured spectrum. Also recall that the spectrum shown in Figure 7 has been produced from an experiment with a pulse repetition frequency far greater than that in a typical multibeam experiment. Furthermore, at high latitudes, probing the ionosphere at large aspect angles relative to **B** means employing beams with low elevation angles and therefore very distant slant ranges to the *F* region altitudes. This results in small signal-to-noise ratios at the receiver. For a phased-array radar, the degradation in performance at low elevation angles is further compounded by the decrease in the antenna effective area at angles away from the boresight, at 55° elevation in the RISR case.

Given the difficulties involved in detecting the non-Maxwellian spectra in a real ISR experiment, it will be insightful to repeat and reexamine the previous studies that sought to perform the standard ISR analysis on non-Maxwellian plasmas while taking into account the statistics of measurements in common programs. In doing so one also needs to include other sources of inaccuracy, for instance, the spatiotemporal ionospheric variability. In Figure 7 the variation of the line-of-sight velocity as a function of range is large and if neglected—for example, by postintegration of the spectrum in range during the fitting procedure—results in the widening and flattening of the ISR spectrum, producing errors similar to those due to non-Maxwellian plasma. Quantitative analysis of these error factors will be the focus of our next study, which targets the issue with simulations from a comprehensive ISR simulator software.

The retrieved ion temperatures from the IPY and Themis experiments presented in the previous section are generally expected to be closer to the actual temperatures than what is suggested by the RISR spectra. This is due to the smaller aspect angle of the radar beams for which the deviation of the one-dimensional distribution function from Maxwellian—and therefore the distortion of the spectrum—is not as critical. Moreover, the amount of error due to integration in range is likely to be reduced as well, since smaller aspect angles translate into smaller coverage over field lines that may possibly contain flows of different magnitudes. On the other hand, the departure of the line-of-sight temperature from the three-dimensional ion temperature will increase. Measuring this departure using the multibeam capability of PFISR/RISR was one of the main goals of this study.

Aspect angle studies of ion temperature in the presence of intense electric fields have been previously carried out by *Winser et al.* [1987, 1989] using EISCAT radars. Their approach was to employ a latitude-scanning experiment where the radar scans the ionosphere over a range of aspect angles in a plane perpendicular to the magnetic L shells. By employing this setup, they were able to identify elevated ion temperature events associated with ion velocities of several kilometer per second and to verify that the line-of-sight ion temperature followed the theoretical predictions of *Raman et al.* [1981]. Prior to that, the anisotropic nature of $F(\boldsymbol{v})$ was also investigated using tristatic EISCAT experiments [*Perraut et al.*, 1984; *Løvhaug and Flå*, 1986] where the three receiver sites measured line-of-sight ion temperature differences of up to 400°K during frictional heating periods. In PFISR experiments we conclude that the difference along the line-of-sight ion temperature for different radar beams is often masked by the spatial variations in $V_{in}$. This is supported by the poor correlation between the predicted and measured $T_{\parallel}$ shown in Figure 11. One approach that could mitigate the spatial-versus-aspect angle ambiguity is to compare ion temperatures at different altitudes that lie on the same magnetic field line, where it is ensured that the measurements are subject to the same ion velocity. Keeping in mind that even then the analysis may be limited by the variations of the neutral wind with altitude, a precise analysis needs to focus on altitudes >280–300 km where the neutral wind is expected to remain constant due to viscosity.

In the context of Figure 11, it is also important to discuss the effect of Coulomb collisions on the ion velocity distribution function. Results from Monte Carlo simulations (as will be presented in a future paper) show that at altitudes above ∼250–300 km and for electric fields of magnitude below 50 mV/m, ion-ion and ion-electron collisions are, in fact, important as they have a noticeable effect in reducing the anisotropy of the ion velocity distribution function. Under such conditions, equation (6) may lose its accuracy. This may be yet another contributing factor to the poor correlation of the expected and measured parallel ion temperature in Figure 11.

Despite the difficulties just described, by utilizing an approach similar to that used to produce Figure 15, the anisotropic nature of the distribution function may still be experimentally quantified in the form of an offset between the theoretical curve of $T_i$ and the measured $T_{i,1d}$. In doing so, one needs to be mindful of the several complicating factors associated with the neutral wind, ion and neutral compositions, and Coulomb collisions. As such, it is critical to separate the analysis based on the altitude of observations. At altitudes below ∼250 km, where the ion and neutral compositions are predominantly $NO^+$ and $N_2$, the polarization interactions dominate the scattering process. On the other hand, for altitudes above ∼300 km the analysis should be based on the assumption of predominantly $O^+$ ions and O neutral particles, and as such, resonant change exchange dominates the scattering process, with some contribution from the polarization interaction. Furthermore, in the latter case and specially for electric field amplitudes <50 mV/m the analysis should also include the role of ion-ion and ion-electron collisions as these become more relevant when the ion temperature is smaller and the plasma density is large.

Making this altitude distinction and provided that the partitioning coefficients $\beta_{\parallel}$ and $\beta_{\perp}$ are known, the line-of-sight ion temperatures in Figure 15 can be adjusted to represent the average temperatures. Shown in Figure 16a are the lower altitude measurements from beam 1 in Figure 15 that are now modified to account for the anisotropic ion distribution based on the partitioning coefficients theoretically derived for the polarization elastic scattering collision model ($\beta_{\parallel} = 0.52$ and $\beta_{\perp} = 0.74$). Overplotted here is the expected ion-neutral differential temperature as a function of the differential flow for three choices of $O/N_2$ composition ratio: 1/2.6, 1/1.35, and 1/0.8. In addition, the dotted line shows the difference between the line-of-sight ion temperatures at the aspect angle of $\varphi = 22.5°$ and the three-dimensional temperatures for the polarization scattering collision model.

Figure 16b shows a similar plot but for the measurements from altitudes ∼300–400 km. The solid theoretical curve is now produced by assuming the neutral composition to be 100% O. Also, the dashed line represents a similar expression as the one in Figure 16a with the exception that this now corresponds to the resonant

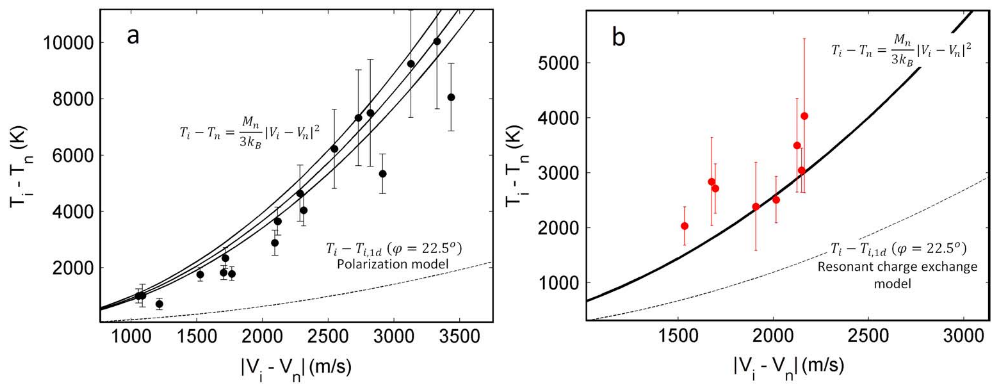


**Figure 16.** The line-of-sight ion temperatures from beam 1 in Figure 15 are separated by the altitude of observations (black circles for measurements from ~130–250 km and red circles for measurements from ~300–400 km) and modified based on the polarization scattering collision model (Figure 16a) and resonant charge exchange collision model (Figure 16b) to represent the three-dimensional ion temperatures. Measurements are then compared with the theoretical curves of $T_i - T_n$ versus $V_{in}$. O/$N_2$ composition ratios of 1/2.6, 1/1.35, 1/0.8 are assumed for the solid curves in Figure 16a, whereas the curve in Figure 16b is produced by assuming 100% O. Finally, the dotted lines show the amount of modification applied to the one-dimensional temperatures in each panel—i.e., they show the expected difference between the line-of-sight ion temperatures at the aspect angle of $\varphi = 22.5°$ and the three-dimensional temperatures according to the appropriate collision models.

charge exchange collision model ($\beta_{\|} = 0.27$ and $\beta_{\perp} = 0.86$). The small number of data points along with their large scatter makes it difficult to comment on the validity of the utilized partitioning coefficients. Nevertheless, it can be seen that the inferred temperatures generally exceed the expected values by up to 1000°K. As will be discussed in a forthcoming paper, about 500°K of this underestimation by the theoretical curve can be attributed to the neglect of Coulomb collisions and their effect in reducing the anisotropy of the distribution function.

In Figure 16 the error bars represent the 1 sigma confidence intervals obtained during the standard ISR fitting procedure. The error estimates for ion velocity are generally low (always below 90 m/s and often closer to 40 m/s) and as such have been removed for the sake of readability of the figure. In addition to such uncertainties, the observed scatter in the data points may also arise from several other sources. One is the possible uncertainty in the assumed neutral composition. Deviation of the neutral composition from output of ionospheric models could arise from changes in the scale height of the neutral atmosphere caused by frictional heating. More important sources of scatter, however, are the neutral winds and the possible inaccuracy in estimating the ion velocity vectors. Provided that the intense ion flows persist over a relatively long period of time, the neutral wind may develop a component along the direction of ion flows through ion drag. Failure to account for this leads to overestimation of the differential flows which could systematically contribute to the departure of the line-of-sight values from the predicted average ion temperatures. In Figure 16a, neutral winds with velocities of several hundred meters per second in the direction of the ion flows may account for the general offset between the data points and the theoretical curves.

Finally, it is important to briefly revisit the troublesome issue of ambiguity in the ion temperature and composition in the standard ISR analysis and to examine our temperature measurements with respect to potential errors due to inaccurate assumption on the ion composition. It is well known that large ion temperatures create a substantial increase in the rate at which $O^+$ ions are converted into $NO^+$ and $O_2^+$ ions [e.g., *St-Maurice and Laneville*, 1998]. This leads to a relatively sudden increase in the proportion of the molecular ions which can be substantial below 300 km altitude [e.g., *Zettergren and Semeter*, 2012]. By increasing the average ion mass, the width of the ion-line spectrum decreases due to decrease in the ion-acoustic speed. If not accounted for in the ISR fitting procedure, this could translate into a substantial underestimation of the ion temperature. The data presented in this study are obtained when the ISR fitting procedure does take into account the ionospheric chemistry. By using for the events of interest an assumed ion composition made of typically greater than 95% molecular ions below 250 km while maintaining a 100% $O^+$ composition ratio above 300 km, we believe that we have stayed clear of potential errors in the retrieval of ion temperatures in relation to erroneous composition assumptions.

Based on the above discussion, we conclude that our proposed modification of the measured line-of-sight temperatures in the bottom side *F* region (130–250 km) based on the partitioning coefficients for the polarization scattering collision model is accurate and necessary when analyzing ISR results of ion temperature during intense frictional heating events. While our conclusions are more tentative for the 300 to 400 km altitude data because of the weaker electric fields involved, there remains the fact that on average the temperature at 22.5° was smaller than at the lower altitudes for similar electric fields and the same aspect angle, which is what we should expect for RCE collisions.

## 5. Summary

Extremely elevated ion temperatures are commonly observed in the *E* and *F* regions of the polar ionosphere by various incoherent scatter radars. Given the dynamic conditions during which the observations are made and the presence of potential sources of error when applying the standard ISR analysis, the measured one-dimensional temperatures—that at times can rise by up to ~8000°K above their quiet time values, inferring average ion temperatures of ~10000°K—are often perceived with uncertainty and skepticism. The most likely sources of error and uncertainty are (1) variability of the plasma flows in spatial and temporal scales unresolved within the often coarse spatial (i.e., range) and temporal integration intervals associated with the ISR fitting procedure, (2) underestimation of the ion temperature at small aspect angles due to anisotropic ion velocity distributions on one hand and its overestimation at large aspect angles due to the non-Maxwellian nature of the distribution function on the other, and (3) underestimation of $T_i$ due to an unanticipated large percentage of molecular ions during periods of intense frictional heating. Eliminating these sources of error is not always straightforward; for instance, accounting for the non-Maxwellian ion distribution at moderate to extreme ion-neutral differential flows is still difficult, owing to the lack of accurate theoretical calculations, which are needed to incorporate the velocity distribution into the ISR fitting procedure. Furthermore, in any realistic scenario all sources of inaccuracy are likely to exist simultaneously and affect the ion temperature estimates at different degrees depending on the experimental setup.

Nevertheless, aiming to clarify the severity of these issues in measurements from the Poker Flat and Resolute Bay ISRs, we have studied the ion temperatures obtained in a number of programs routinely run by these radars. By comparing the measured one-dimensional ion temperatures from many events with the average ion temperature values that are expected from frictional heating and ion flows that are simultaneously estimated by the radar, we find that at altitudes of ~130–250 km, where the ion and neutral particles are predominantly $NO^+$, $N_2$, and O, $T_{i,1d}$ at the aspect angle 22.5° is lower than $T_i$ by an amount that matches well with the theoretically expected value from a polarization elastic scattering collision model. These results are the clearest detection of anisotropic ion velocity distributions with the PFISR and RISR facilities.

The excellent match between theory and observations is possible below 250 km since (as confirmed with our new Monte Carlo calculations) the standard ISR analysis based on the Maxwellian ion distribution would generally produce an accurate estimation of $T_{i,1d}$ for the $NO^+$-$N_2$ plasma at these altitudes, even when the distribution function deviates from isotropic Maxwellian.

Our attempts to detect the aspect angle dependence of the line-of-sight ion temperature in multibeam experiments failed. This is mainly due to the fact that the differences in $T_{i,1d}$ at different aspect angles are masked by the more important spatial variations of the ion-neutral differential flows and the limitations of PFISR and RISR in providing accurate point measurements of the vector quantities. While the EISCAT tristatic capability is more suitable for such studies, these limitations of PFISR/RISR may also be managed via specially designed experiments—for instance, by employing clusters of closely located beams at different aspect angles in order to obtain more localized and accurate estimates of the flows or by monitoring the ion temperatures on the same magnetic field lines, though at different altitudes, where the flows are known to be constant. Accurate determination of the partitioning coefficients as a function of altitude could be a useful outcome of such experiments.

At the aspect angle of 55° and for an event where the ion temperature and the field-perpendicular ion velocity at 300–450 km reached to the high values of ~8000°K and ~4 km/s, respectively, we were able to identify ISR spectra that resemble those theoretically expected from non-Maxwellian ion distributions. Although for this particular case the spectra contained a relatively moderate level of noise-like fluctuations, the amount of fluctuations is only expected to increase in a typical PFISR/RISR experiment that includes a large number of radar beams. Large fluctuations could mask the moderate differences between the spectra from Maxwellian and non-Maxwellian plasmas. Any analysis to determine the amount of error in the measured plasma parameters in these situations should be broadened to include such fluctuations as well as the spatiotemporal variability of the ionosphere when the integration periods are as long as several minutes. We intend to address this issue quantitatively using a forthcoming ISR simulator capable of fully modeling a realistic PFISR/RISR experiment.

**Acknowledgments**
This work was supported by the National Science Foundation under grant AGS-1339500 and by the Air Force Office of Sponsored Research under contract FA9550-15-1-0503. J.P.S.M. and L.V.G. were supported by NSERC and the Canada Research Chair program. The data employed in this study are publicly accessible from the PFISR/RISR databases at http://amisr.sri.com/database/ or by contacting this manuscript's corresponding author (hakbari@bu.edu).

## References

Barakat, A., R. Schunk, and J. St-Maurice (1983), Monte-Carlo calculations of the $O^+$ velocity distributions in the auroral ionosphere, *J. Geophys. Res*, *88*, 3237–3241.

Baron, M. J., and R. H. Wand (1983), *F* region ion temperature enhancements resulting from Joule heating, *J. Geophys. Res.*, *88*(A5), 4114–4118.

Bernhardt, P., J. Huba, W. Swartz, and M. Kelley (1998), Incoherent scatter from space shuttle and rocket engine plumes in the ionosphere, *J. Geophys. Res.*, *103*(A2), 2239–2251.

Davies, J., M. Lester, B. Jenkins, and R. Moffett (1995), Dayside ion frictional heating: EISCAT observations and comparison with model results, *J. Atmos. Terr. Phys.*, *57*(7), 775–793.

Davies, J., M. Lester, and I. McCrea (1999), Solar and seasonal dependence of ion frictional heating, *Ann. Geophys.*, *17*, 682–691.

Gaimard, P., J.-P. St-Maurice, C. Lathuillere, and D. Hubert (1998), On the improvement of analytical calculations of collisional auroral ion velocity distributions using recent Monte Carlo results, *J. Geophys. Res.*, *103*(A3), 4079–4095.

Hagan, M. E., and D. P. Sipler (1991), Combined incoherent scatter radar and Fabry-Perot interferometer measurements of frictional heating effects over Millstone Hill during March 7–10, 1989, *J. Geophys. Res.*, *96*(A1), 289–296.

Heinselman, C. J., and M. J. Nicolls (2008), A Bayesian approach to electric field and *E*-region neutral wind estimation with the Poker Flat Advanced Modular Incoherent Scatter Radar, *Radio Sci.*, *43*, RS5013, doi:10.1029/2007RS003805.

Lockwood, M., and T. Fuller-Rowell (1987), The modelled occurrence of non-thermal plasma in the ionospheric *F*-region and the possible consequences for ion outflows into the magnetosphere, *Geophys. Res. Lett.*, *14*(4), 371–374.

Lockwood, M., B. Bromage, R. Horne, J.-P. St-Maurice, D. Willis, and S. Cowley (1987), Non-Maxwellian ion velocity distributions observed using EISCAT, *Geophys. Res. Lett.*, *14*(2), 111–114.

Lockwood, M., K. Suvanto, K. Winser, S. Cowley, and D. Willis (1989), Incoherent scatter radar observations of non-Maxwellian ion velocity distributions in the auroral *F*-region, *Adv. Space Res.*, *9*(5), 113–118.

Lockwood, M., S. Cowley, P. Sandholt, and R. Lepping (1990), The ionospheric signatures of flux transfer events and solar wind dynamic pressure changes, *J. Geophys. Res.*, *95*(A10), 17,113–17,135.

Løvhaug, U., and T. Flå (1986), Ion temperature anisotropy in the auroral *F*-region as measured with EISCAT, *J. Atmos. Terr. Phys.*, *48*(9), 959–971.

Lyons, L., Y. Nishimura, Y. Shi, S. Zou, H.-J. Kim, V. Angelopoulos, C. Heinselman, M. Nicolls, and K.-H. Fornacon (2010), Substorm triggering by new plasma intrusion: Incoherent-scatter radar observations, *J. Geophys. Res.*, *115*, A07223, doi:10.1029/2009JA015168.

Moorcroft, D., and K. Schlegel (1988), Evidence for non-Maxwellian ion velocity distributions in the *F*-region, *J. Atmos. Terr. Phys.*, *50*(4), 455–465.

Nicolls, M. J., M. C. Kelley, A. J. Coster, S. A. González, and J. J. Makela (2004), Imaging the structure of a large-scale TID using ISR and TEC data, *Geophys. Res. Lett.*, *31*, L09812, doi:10.1029/2004GL019797.

Perraut, S., A. Brekke, M. Baron, and D. Hubert (1984), EISCAT measurements of ion temperatures which indicate non-isotropic ion velocity distributions, *J. Atmos. Terr. Phys.*, *46*(6), 531–543.

Raman, R., J. St-Maurice, and R. Ong (1981), Incoherent scattering of radar waves in the auroral ionosphere, *J. Geophys. Res.*, *86*(A6), 4751–4762.

Schunk, R., W. Raitt, and P. Banks (1975), Effect of electric fields on the daytime high-latitude *E* and *F* regions, *J. Geophys. Res.*, *80*(22), 3121–3130.

Semeter, J., T. Butler, C. Heinselman, M. Nicolls, J. Kelly, and D. Hampton (2009), Volumetric imaging of the auroral ionosphere: Initial results from PFISR, *J. Atmos. Sol. Terr. Phys.*, *71*, 738–743, doi:10.1016/j.JASTP.2008.08.014.

St.-Maurice, J.-P., and W. Hanson (1982), Ion frictional heating at high latitudes and its possible use for an in situ determination of neutral thermospheric winds and temperatures, *J. Geophys. Res.*, *87*(A9), 7580–7602.

St-Maurice, J.-P. (1978), On a mechanism for the formation of VLF electrostatic emissions in the high latitude *F*-region, *Planet. Space Sci.*, *26*(9), 801–816.

St-Maurice, J.-P., and R. Schunk (1977), Auroral ion velocity distributions for a polarization collision model, *Planet. Space Sci.*, *25*(3), 243–260.

St-Maurice, J.-P., and R. Schunk (1979), Ion velocity distributions in the high-latitude ionosphere, *Rev. Geophys.*, *17*(1), 99–134.

St.-Maurice, J.-P., W. Hanson, and J. Walker (1976), Retarding potential analyzer measurement of the effect of ion-neutral collisions on the ion velocity distribution in the auroral ionosphere, *J. Geophys. Res.*, *81*, 5438–5446.

St-Maurice, J.-P. S., and P. Laneville (1998), Reaction rate of $O^+$ with $O_2$, $N_2$, and NO under highly disturbed auroral conditions, *J. Geophys. Res.*, *17*(A8), 519–517.

Suvanto, K. (1987), Auroral *F*-region ion velocity distributions in the presence of large flows and electrostatic waves, *Planet. Space Sci.*, *35*(11), 1429–1435.

Suvanto, K. (1988), Incoherent scattering of radar waves from nonthermal *F* region plasma: Analytical methods of spectrum synthesis, *Radio Sci.*, *23*(6), 989–996.

Suvanto, K. (1990a), On the analysis of incoherent scatter radar data from non-thermal ionospheric plasma: Effects of measurement noise and an inexact theory, *Planet. Space Sci.*, *38*(7), 903–912.

Suvanto, K. (1990b), Microinstabilities driven by non-thermal plasma in the high-latitude *F*-region, *Adv. Space Res.*, *10*(6), 149–152.

Suvanto, K., M. Lockwood, K. Winser, A. Farmer, and B. Bromage (1989), Analysis of incoherent scatter radar data from non-thermal *F*-region plasma, *J. Atmos. Terr. Phys.*, *51*(6), 483–495.

Todd, H., B. Bromage, S. Cowley, M. Lockwood, A. Van Eyken, and D. Willis (1986), EISCAT observations of bursts of rapid flow in the high latitude dayside ionosphere, *Geophys. Res. Lett.*, *13*(9), 909–912.

Winkler, E., J. St-Maurice, and A. Barakat (1992), Results from improved Monte Carlo calculations of auroral ion velocity distributions, *J. Geophys. Res.*, *97*, 8399–8423.

Winser, K. J., M. Lockwood, and G. O. L. Jones (1987), Non-thermal plasma observations using EISCAT: Aspect angle dependence, *Geophys. Res. Lett.*, *14*(9), 957–960.

Winser, K., M. Lockwood, G. Jones, and K. Suvanto (1989), Radar observations of non-thermal plasmas at different aspect angles, *Adv. Space Res.*, *9*(5), 107–112.

Zettergren, M., and J. Semeter (2012), Ionospheric plasma transport and loss in auroral downward current regions, *J. Geophys. Res.*, *117*, A06306, doi:10.1029/2012JA01763.

Zettergren, M., J. Semeter, B. Burnett, W. Oliver, C. Heinselman, M. Díaz Beneventi, and P.-L. Blelly (2010), Dynamic variability in *F*-region ionospheric composition at auroral arc boundaries, *Ann. Geophys.*, *28*, 651–664.

Zettergren, M., J. Semeter, C. Heinselman, and M. Diaz (2011), Incoherent scatter radar estimation of F region ionospheric composition during frictional heating events, *J. Geophys. Res.*, *116*, A01318, doi:10.1029/2010JA016035.

Zou, S., L. Lyons, M. Nicolls, and C. Heinselman (2009), PFISR observations of strong azimuthal flow bursts in the ionosphere and their relation to nightside aurora, *J. Atmos. Sol. Terr. Phys.*, *71*(6), 729–737.